

Josephson effect in a multi-orbital model for Sr_2RuO_4

Kohei Kawai

Department of Applied Physics, Nagoya University, Nagoya 464-8603, Japan

Keiji Yada and Yukio Tanaka

*Department of Applied Physics, Nagoya University, Nagoya 464-8603, Japan,
Moscow Institute of Physics and Technology, Dolgoprudny, Moscow 141700, Russia*

Yasuhiro Asano

*Department of Applied Physics, Hokkaido University, Sapporo 060-8628, Japan,
Moscow Institute of Physics and Technology, Dolgoprudny, Moscow 141700, Russia*

Alexander A. Golubov

*Faculty of Science and Technology and MESA+ Institute of Nanotechnology,
University of Twente, 7500 AE, Enschede, The Netherlands,
Moscow Institute of Physics and Technology, Dolgoprudny, Moscow 141700, Russia*

Satoshi Kashiwaya

*National Institute of Advanced Industrial Science and Technology (AIST), Tsukuba 305-8568,
Japan, Moscow Institute of Physics and Technology, Dolgoprudny, Moscow 141700, Russia*

(Dated: September 4, 2018)

We study Josephson currents between s -wave/spin-triplet superconductor junctions by taking into account details of the band structures in Sr_2RuO_4 , such as three conduction bands and spin-orbit interactions in the bulk and at the interface. We assume five superconducting order parameters in Sr_2RuO_4 : a chiral p -wave symmetry and four helical p -wave symmetries. We calculate the current-phase relationship $I(\varphi)$ in these junctions, where φ is the macroscopic phase difference between the two superconductors. The results for a chiral p -wave pairing symmetry show that a $\cos(\varphi)$ term appears in the current-phase relation because of time-reversal symmetry (TRS) breaking. On the other hand, this $\cos(\varphi)$ term is absent in the helical pairing states that preserve TRS. We also study the dependence of the maximum Josephson current I_c on an external magnetic flux Φ in a corner junction. The calculated $I_c(\Phi)$ obeys $I_c(\Phi) \neq I_c(-\Phi)$ in a chiral state and $I_c(\Phi) = I_c(-\Phi)$ in a helical state. We calculate $I_c(\Phi)$ in a corner SQUID and a symmetric SQUID geometry. In the latter geometry, $I_c(\Phi) = I_c(-\Phi)$ is satisfied for all the pairing states and it is impossible to distinguish a chiral state from a helical one. On the other hand, a corner SQUID always gives $I_c(\Phi) \neq I_c(-\Phi)$ and $I_c(\Phi) = I_c(-\Phi)$ for a chiral and a helical state, respectively. Experimental tests of these relations in corner junctions and SQUIDs may serve as a tool for unambiguously determining the pairing symmetry in Sr_2RuO_4 .

I. INTRODUCTION

Strontium ruthenate (Sr_2RuO_4 , or SRO) has attracted much interest for its unconventional superconductivity below the critical temperature $T_c \sim 1.5 \text{ K}$. The constancy of the Knight shift across T_c is strongly indicative of spin-triplet pairing order²⁻⁶. Many theoretical studies have examined the microscopic mechanism of spin-triplet pairings in this material⁷⁻²¹. Exotic phenomena specific to spin-triplet superconductors²²⁻²⁶ are therefore naturally expected in SRO. Although several studies have focused on the superconducting order parameter, the symmetry of a Cooper pair is not yet fully understood. Five spin-triplet pairing states are compatible with the tetragonal crystal structure of SRO⁵. One of these is a spin-triplet chiral p -wave state (denoted the E_u state in the Mulliken notation) where the d -vector is parallel to c -axis of the crystal. The other four candidates are called spin-triplet helical states (denoted A_{1u} , A_{2u} , B_{1u} , and B_{2u} in the Mulliken notation), where the d -vectors lie in the

ab -plane of the crystal.

According to the recently proposed topological classification²⁷⁻³⁰, all of the proposed superconducting states are topologically nontrivial. Consequently, topologically protected Andreev bound states are expected at an SRO surface³¹. Some experimental results are consistent with the proposed pair potential. It has been suggested that the maximum Josephson current in $\text{Au}_{0.5}\text{In}_{0.5}$ -SRO superconducting quantum interference devices (SQUID) displays an odd-parity pairing state³².

Tunneling spectroscopy experiments also suggest the formation of a dispersive surface Andreev bound state (SABS) at the in-plane edges of SRO^{31,33,34}. The dispersive SABSs^{35,36} are distinguishable from the dispersionless SABS in a d -wave superconductor. The former generates a broad zero-bias conductance peak (ZBCP)³⁷⁻³⁹, whereas the latter forms a sharp ZBCP⁴⁰⁻⁴². Because SRO is a multi-band superconductor, the numerically determined energy dispersion of an SABS in a multi-band model is more complicated than that in a single-orbital

model^{43,44}. Yada, *et al.* successfully explained the variety of conductance spectra observed in experiments³¹ in terms of the three-band degrees of freedom⁴⁵. Several Josephson-junction experiments suggested the presence of domain structures, detected from an anomalous current-switching behavior^{46–50}. These experimental findings are consistent with the existence of both chiral and helical p -wave pairing symmetries in SRO.

A chiral state is qualitatively different from the four helical states because it breaks the time-reversal symmetry (TRS), whereas the helical states preserve TRS⁵¹. Although the presence or absence of TRS in SRO is an important issue, experimental results remain controversial. TRS breaking can be verified by observing a spontaneous magnetic field or a spontaneous edge current. Theoretical studies have shown that the amplitude of the spontaneous magnetization is detectable experimentally⁵² and that the edge current is robust with respect to surface roughness⁵³. Measurements of muon spin resonance and of the Kerr effect have detected the presence of an internal magnetic field^{54,55}, which in turn suggests a chiral p -wave symmetry. On the other hand, scanning SQUID experiments have not shown any signs of a spontaneous magnetic field^{56,57}, which suggests a helical p -wave symmetry. Several theoretical proposals have been put forward to explain the absence of the edge current in SRO^{17,58–61}. A resolution of this paradox requires an experimental test able to distinguish unambiguously between a chiral and a helical pairing symmetry.

In this paper, we present a theory of the Josephson effect between a spin-singlet s -wave superconductor and a spin-triplet p -wave superconductor by taking into account the three bands of the SRO in addition to the spin-orbit interaction in the bulk and at the interface. The importance of multi-orbital effects are apparent in various physical quantities^{15,62}. Since spin-orbit coupling influences the current-phase relation fundamentally, it is necessary that our theory consider a three-band model. We calculated the current-phase relation $I(\varphi)$ in Josephson junctions, where φ is the macroscopic phase difference between the two superconductors. We found that $\cos(\varphi)$ appears in $I(\varphi)$ for chiral p -wave pairing, owing to TRS breaking, to ensure consistency with previous results⁶³. However, $\cos(\varphi)$ is absent for helical pairing, thus reflecting time-reversal invariance. In the case of helical pairing, $\sin(\varphi)$ appears only in a three-band model. We also studied the dependence of the maximum Josephson current I_c on an external magnetic flux Φ in two types of SQUID geometries: a corner SQUID and a symmetric SQUID. In a corner Josephson junction and a corner SQUID, we found $I_c(\Phi) \neq I_c(-\Phi)$ for a chiral state, whereas $I_c(\Phi) = I_c(-\Phi)$ holds true for a helical state. We show that the three-band character affects the oscillation period of $I_c(\Phi)$. It is possible to determine the pairing symmetry unambiguously by testing these relations in SRO-based corner junctions and SQUIDS. In a symmetric SQUID, the relation $I_c(\Phi) = I_c(-\Phi)$ is satisfied in both chiral and helical cases.

II. MODEL AND FORMULATIONS

This section introduces a model Hamiltonian for an SRO/normal metal (NM)/ s -wave superconductor junction system. First, we explain the Hamiltonian for bulk SRO, which consists of three terms \mathcal{H}_{kin} , \mathcal{H}_{soi} and $\mathcal{H}_{\text{pair}}$. The first term \mathcal{H}_{kin} expresses the kinetic energy. ARPES measurements and first-principles calculations have shown that SRO has three two-dimensional Fermi surfaces^{64–67}. These Fermi surfaces were reproduced by considering three orbitals, *i.e.*, the d_{xy} , d_{yz} , and d_{zx} orbitals, in SRO. We can therefore consider a three-band two-dimensional Hamiltonian constructed using the tight-binding model:

$$\mathcal{H}_{\text{kin}} = \sum_{\mathbf{k}, \sigma} \hat{c}_{\mathbf{k}\sigma}^\dagger \begin{pmatrix} \varepsilon_{yz}(\mathbf{k}) & g(\mathbf{k}) & 0 \\ g(\mathbf{k}) & \varepsilon_{zx}(\mathbf{k}) & 0 \\ 0 & 0 & \varepsilon_{xy}(\mathbf{k}) \end{pmatrix} c_{\mathbf{k}\sigma}, \quad (1)$$

where \mathbf{k} is a wavenumber, σ is the spin, and $\hat{c}_{\mathbf{k}\sigma} = (c_{\mathbf{k},\sigma}^{yz}, c_{\mathbf{k},\sigma}^{zx}, c_{\mathbf{k},-\sigma}^{xy})^T$ is the annihilation operator. The matrix components of Eq. (1) are given by

$$\varepsilon_{xy}(\mathbf{k}) = -2t_1(\cos k_x + \cos k_y) - 4t_2 \cos k_x \cos k_y - \mu_{xy}, \quad (2)$$

$$\varepsilon_{yz}(\mathbf{k}) = -2t_4 \cos k_x - 2t_3 \cos k_y - \mu_{yz}, \quad (3)$$

$$\varepsilon_{zx}(\mathbf{k}) = -2t_3 \cos k_x - 2t_4 \cos k_y - \mu_{zx}, \quad (4)$$

$$g(\mathbf{k}) = -4t_5 \sin k_x \sin k_y, \quad (5)$$

where t_1 , t_2 , t_3 , t_4 , and t_5 are the hopping integrals up to next nearest-neighbor sites. The second term \mathcal{H}_{soi} denotes the spin-orbit interaction in bulk SRO,

$$\mathcal{H}_{\text{soi}} = \lambda \sum_{\mathbf{k}, \sigma} \hat{c}_{\mathbf{k}\sigma}^\dagger \begin{pmatrix} 0 & is_\sigma & -s_\sigma \\ -is_\sigma & 0 & i \\ -s_\sigma & -i & 0 \end{pmatrix} \hat{c}_{\mathbf{k}\sigma}, \quad (6)$$

where $s_\sigma = 1$ ($s_\sigma = -1$) for $\sigma = \uparrow$ ($\sigma = \downarrow$). This term mixes the spin and orbital degrees of freedom. The third term $\mathcal{H}_{\text{pair}}$ expresses the pair potential in SRO. We chose spin-triplet chiral and helical p -wave pairings in the following analysis. In the chiral p -wave case, we considered a pair potential which belongs to the E_u irreducible representation. In the helical p -wave case, we considered two kinds of pair potentials belonging to the A_u and B_u irreducible representations. Using the orbital-dependent d vector $d^\ell(\mathbf{k})$, the pair potential can be expressed as

$$\mathcal{H}_{\text{pair}} = \sum_{\ell} \hat{c}^{\ell\dagger} \begin{pmatrix} \hat{0} & \hat{\Delta}^\ell(\mathbf{k}) \\ -\hat{\Delta}^{\ell*}(-\mathbf{k}) & \hat{0} \end{pmatrix} \hat{c}^\ell, \quad (7)$$

with $\hat{c}^\ell = (c_{\mathbf{k},\uparrow}^\ell, c_{\mathbf{k},\downarrow}^\ell, c_{-\mathbf{k},\uparrow}^{\ell\dagger}, c_{-\mathbf{k},\downarrow}^{\ell\dagger})^T$, and $\hat{\Delta}^\ell(\mathbf{k}) = id^\ell(\mathbf{k}) \cdot \boldsymbol{\sigma}_y$, where ℓ denotes the orbital index. The five kinds

of d vectors are given by

$$\begin{cases} \mathbf{d}_{Eu}^{yz} = \hat{z}\Delta_1(\delta \sin k_x + i \sin k_y), \\ \mathbf{d}_{Eu}^{zx} = \hat{z}\Delta_1(\sin k_x + i\delta \sin k_y), \\ \mathbf{d}_{Eu}^{xy} = \hat{z}\Delta_2(\sin k_x + i \sin k_y), \end{cases} \quad (8)$$

$$\begin{cases} \mathbf{d}_{A1u}^{yz} = \hat{x}\delta\Delta_1 \sin k_x + \hat{y}\Delta_1 \sin k_y, \\ \mathbf{d}_{A1u}^{zx} = \hat{x}\Delta_1 \sin k_x + \hat{y}\delta\Delta_1 \sin k_y, \\ \mathbf{d}_{A1u}^{xy} = \hat{x}\Delta_2 \sin k_x + \hat{y}\Delta_2 \sin k_y, \end{cases} \quad (9)$$

$$\begin{cases} \mathbf{d}_{A2u}^{yz} = \hat{x}\Delta_1 \sin k_y - \hat{y}\delta\Delta_1 \sin k_x, \\ \mathbf{d}_{A2u}^{zx} = \hat{x}\delta\Delta_1 \sin k_y - \hat{y}\Delta_1 \sin k_x, \\ \mathbf{d}_{A2u}^{xy} = \hat{x}\Delta_2 \sin k_y - \hat{y}\Delta_2 \sin k_x, \end{cases} \quad (10)$$

$$\begin{cases} \mathbf{d}_{B1u}^{yz} = \hat{x}\Delta_1 \sin k_x - \hat{y}\delta\Delta_1 \sin k_y, \\ \mathbf{d}_{B1u}^{zx} = \hat{x}\delta\Delta_1 \sin k_x - \hat{y}\Delta_1 \sin k_y, \\ \mathbf{d}_{B1u}^{xy} = \hat{x}\Delta_2 \sin k_x - \hat{y}\Delta_2 \sin k_y, \end{cases} \quad (11)$$

$$\begin{cases} \mathbf{d}_{B2u}^{yz} = \hat{x}\delta\Delta_1 \sin k_y + \hat{y}\Delta_1 \sin k_x, \\ \mathbf{d}_{B2u}^{zx} = \hat{x}\Delta_1 \sin k_y + \hat{y}\delta\Delta_1 \sin k_x, \\ \mathbf{d}_{B2u}^{xy} = \hat{x}\Delta_2 \sin k_y + \hat{y}\Delta_2 \sin k_x. \end{cases} \quad (12)$$

In these pair potentials, we only considered the intra-orbital pairing cases. Furthermore, we introduced anisotropy in the pair potential in quasi-one-dimensional d_{yz} and d_{zx} orbitals by setting $\delta < 1$. In addition, the crystalline symmetry of SRO allows different magnitudes of the pair potential for the two-dimensional d_{yz} orbital (Δ_1) and the quasi-one-dimensional d_{yz} and d_{zx} orbitals (Δ_2).

In the NM region between an SRO and an s -wave superconductor, we considered a single-orbital model given by

$$\mathcal{H}_{\text{NM}} = \sum_{\mathbf{k}\sigma} (\varepsilon_{\mathbf{k}} - \mu) c_{\mathbf{k}\sigma}^\dagger c_{\mathbf{k}\sigma}, \quad (13)$$

where $c_{\mathbf{k}\sigma}$ is the annihilation operator for an electron in the NM. The energy dispersion of the NM is given by

$$\varepsilon_{\mathbf{k}} = -2t_1(\cos(k_x) + \cos(k_y)) - 4t_2 \cos(k_x) \cos(k_y) - \mu_n$$

where t is the hopping integral between nearest-neighbor sites. We took into account the interface Rashba spin-orbit coupling in the NM layer next to the SRO, which is given by

$$\mathcal{H}_{\text{RSOI}} = \lambda_R \sin k_y \hat{\sigma}_z. \quad (14)$$

In the spin-singlet s -wave superconductor region, we considered the on-site pair potential as well as the kinetic-energy term in Eq. (13):

$$\mathcal{H}_{s\text{-wave}} = \sum_{\mathbf{k}} \Delta e^{i\varphi} c_{\mathbf{k}\uparrow}^\dagger c_{-\mathbf{k}\downarrow}^\dagger + \text{c.c.}, \quad (15)$$

where φ is the macroscopic phase of the pair potential relative to the interface normal of the p -wave superconductor. These three parts are coupled via hopping at

the interface. The magnitude of the hopping at the interface between the NM and the s -wave superconductor was chosen to be the same as in the NM. The SRO-NM interface displays three kinds of hopping: t_{xy} , t_{yz} , and t_{zx} . The first, t_{xy} , corresponds to the hopping between the NM and the d_{xy} orbital of SRO. Likewise, t_{yz} (t_{zx}) also denotes the interface hopping between NM and d_{yz} (d_{zx}) orbital of SRO.

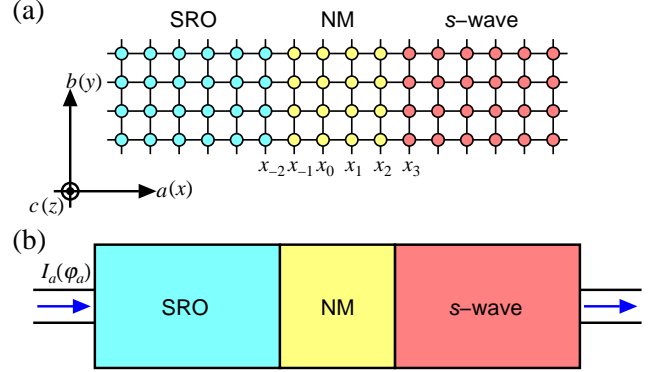


FIG. 1. (a) Lattice model of the junction considered in this paper. (b) Schematic illustrations of an SRO (Sr_2RuO_4)/NM (normal metal) / s -wave superconductor single Josephson junction.

We calculated the current-phase relation of the Josephson current in the single junction (see FIG. 1. (a)) based on a lattice Green's function method that takes into account the Andreev reflection and Andreev bound states at the interface^{68,69}. For that purpose, we calculated the Green's function in the superconducting SRO/NM/ s -wave superconductor junction. These three regions are aligned in the (100) direction, with the boundaries for the s -wave superconductor and SRO located at $x \leq x_{-2}$ and $x \geq x_3$, respectively. In the numerical calculations, four NM layers are inserted between these two superconductors at $x_{-1} \leq x \leq x_2$. Since we are considering flat interfaces in the ballistic limit, k_y is a conserved quantity. In order to obtain the Green's function in this junction, we first calculated the surface Green's functions of the semi-infinite SRO and spin-singlet s -wave superconductor, where the surfaces are not coupled to the NM layer. These calculations were based on the recursive Green's function method, using Möbius transformation⁷⁰. Next, we added the two NM layers on these surfaces with the following recursive equation:

$$\hat{G}_n^L(k_y, i\omega_l) = (i\omega_l - \hat{\varepsilon}_n(k_y) - \hat{t}_{n,n-1} \hat{G}_{n-1}^L(k_y, i\omega_l) \hat{t}_{n-1,n})^{-1}, \quad (16)$$

$$\hat{G}_n^R(k_y, i\omega_l) = (i\omega_l - \hat{\varepsilon}_n(k_y) - \hat{t}_{n,n+1} \hat{G}_{n+1}^L(k_y, i\omega_l) \hat{t}_{n+1,n})^{-1}, \quad (17)$$

where $G_n^{LI}(k_y, i\omega_l)$ stands for the surface Green's function for the system on the left (right) side of the interface, with $x \leq x_n$ ($x \geq x_n$). The operators $\hat{\varepsilon}_n(k_y)$ and $\hat{t}_{n,n-1}$

represent the local and non-local parts of the Hamiltonian. Then, we obtained two surface Green's function, defined for $x \leq x_0$ and $x \geq x_1$. These two systems are combined in the equation

$$\hat{G}_{00}(k_y, i\omega_l) = ((\hat{G}_0^L(k_y, i\omega_l))^{-1} - \hat{t}_{01}\hat{G}_1^R(k_y, i\omega_l)\hat{t}_{10})^{-1}, \quad (18)$$

$$\hat{G}_{11}(k_y, i\omega_l) = ((\hat{G}_1^R(k_y, i\omega_l))^{-1} - \hat{t}_{10}\hat{G}_0^L(k_y, i\omega_l)\hat{t}_{01})^{-1}. \quad (19)$$

Then, we obtained the non-local Green's functions in the s -wave/NM/SRO junction as follows:

$$\hat{G}_{01}(k_y, i\omega_l) = \hat{G}_0^L(k_y, i\omega_l)\hat{t}_{01}\hat{G}_{11}(k_y, i\omega_l) \quad (20)$$

$$\hat{G}_{10}(k_y, i\omega_l) = \hat{G}_1^R(k_y, i\omega_l)\hat{t}_{10}\hat{G}_{00}(k_y, i\omega_l). \quad (21)$$

The Fourier-transforms of $\hat{G}_{01}(k_y, i\omega_l)$ and $\hat{G}_{10}(k_y, i\omega_l)$ are given by

$$\hat{G}_{01}(k_y, \tau) = \frac{1}{\beta} \sum_l \hat{G}_{01}(k_y, i\omega_l) e^{-i\omega_l \tau} \quad (22)$$

$$\hat{G}_{10}(k_y, \tau) = \frac{1}{\beta} \sum_l \hat{G}_{10}(k_y, i\omega_l) e^{-i\omega_l \tau}. \quad (23)$$

with $\beta = 1/(k_B T)$ and where T is the temperature. The above formulas for $\hat{G}_{01}(k_y, \tau)$ and $\hat{G}_{10}(k_y, \tau)$ can be expressed as

$$\hat{G}_{01}(k_y, \tau) = - \left\langle T_\tau \left[\hat{C}_0(\tau) \hat{C}_1^\dagger \right] \right\rangle \quad (24)$$

$$\hat{G}_{10}(k_y, \tau) = - \left\langle T_\tau \left[\hat{C}_1(\tau) \hat{C}_0^\dagger \right] \right\rangle, \quad (25)$$

with

$$\hat{C}_0^\dagger = \begin{pmatrix} C_{0e\uparrow}^\dagger & C_{0e\downarrow}^\dagger & C_{0h\uparrow}^\dagger & C_{0h\downarrow}^\dagger \end{pmatrix} \quad (26)$$

$$\hat{C}_1^\dagger = \begin{pmatrix} C_{1e\uparrow}^\dagger & C_{1e\downarrow}^\dagger & C_{1h\uparrow}^\dagger & C_{1h\downarrow}^\dagger \end{pmatrix}. \quad (27)$$

Thus, we obtained the current-phase relation $I(\varphi)$ by using these $\hat{G}_{01}(k_y, \tau)$ and $\hat{G}_{10}(k_y, \tau)$:

$$\begin{aligned} I(\varphi) &= \frac{i e t}{\hbar} \int_{-\pi}^{\pi} \text{Tr}' \left[\hat{G}_{01}(k_y, \tau = -0, \varphi) \right. \\ &\quad \left. - \hat{G}_{10}(k_y, \tau = -0, \varphi) \right] dk_y \\ &= \frac{i e t}{\hbar} \int_{-\pi}^{\pi} \text{Tr}' \frac{1}{\beta} \sum_l \left[\hat{G}_{01}(k_y, i\omega_l, \varphi) \right. \\ &\quad \left. - \hat{G}_{10}(k_y, i\omega_l, \varphi) \right] dk_y, \quad (28) \end{aligned}$$

where Tr' is a partial sum of the diagonal elements of the Hamiltonian, including only those matrix elements that refer to the electron space.

Below, we define the model parameters that were used in the calculations. For the hopping parameters in SRO, we assumed $t_2/t_1 = 0.395$, $t_3/t_1 = 1.25$, $t_4/t_1 = 0.125$, and $t_5/t_1 = 0.15$, based on first-principles calculations.

Here, t_1 is the nearest-neighbor hopping parameter in the d_{xy} orbital in SRO, which first-principles calculations estimate as being approximately 230 meV⁵. Furthermore, the chemical potentials in each orbital in SRO, μ_{yz} , μ_{zx} , and μ_{xy} , were chosen to yield the following numbers of electron: $n_{yz} = n_{zx} = n_{xy} = 2/3$. The chemical potential in the normal metal, μ_n , was chosen so that the number of electron is 2/3. The magnitude of the spin-orbit interaction in the bulk SRO, expressed as λ , changes these values. We set $\lambda = 0.3$ for consistency with quasiparticle spectra obtained by angle-resolved photoemission spectroscopy⁵. We chose the magnitudes of the pair potential for the d_{yz} and d_{zx} orbitals in SRO to exceed that of the d_{xy} orbital, as determined previously by tunneling spectroscopy^{31,45}. The magnitude of the pair potential in the d_{yz} and d_{zx} orbitals was set to $\Delta_1 = 0.001t_1$. We set the magnitude of the pair potential for the d_{xy} -orbital to $\Delta_2 = 0.4\Delta_1$. For the quasi-one-dimensional nature of the pair potential for d_{xy} -orbital, we set $\delta = 0.1$, based on the ratio of t_3 to t_4 .

We assumed that an s -wave superconductor and an NM are described by the same single-orbital model as that of the d_{xy} orbital in SRO. We set their chemical potentials μ_n to the same level as the d_{xy} orbital in SRO, in the absence of spin-orbit interaction in the bulk SRO. The magnitude of the pair potential of the s -wave superconductor was set to $\Delta_s = 10\Delta_1$. The magnitude of the Rashba spin-orbit interaction at the interface between NM and SRO, λ_R , depends on the microscopic electronic properties of the junction and was set to 0.3 in this study.

III. RESULTS

A. current phase relation

Figure 2 shows the current-phase relation in the absence of interface Rashba spin-orbit interaction. Here, the Josephson current $I(\varphi)$ is decomposed into the Fourier series

$$I(\varphi) = \sum_{n=1}^{\infty} I_n^s \sin(n\varphi) + I_n^c \cos(n\varphi). \quad (29)$$

It is then normalized by I_0 , the maximum value of the Fourier coefficients. Table I shows which of the Fourier coefficients have nonzero values.

	I_1^s	I_1^c	I_2^s	I_2^c
(a) Chiral(single-band)	—	—	✓	—
(b) Chiral(multi-band)	✓	✓	✓	✓
(c) Helical(single-band)	—	—	✓	—
(d) Helical(multi-band)	✓	—	✓	—

TABLE I. Fourier series of current-phase relation in the absence of interface Rashba spin-orbit interaction. ✓ (—) denotes coefficients with a nonzero (zero) value.

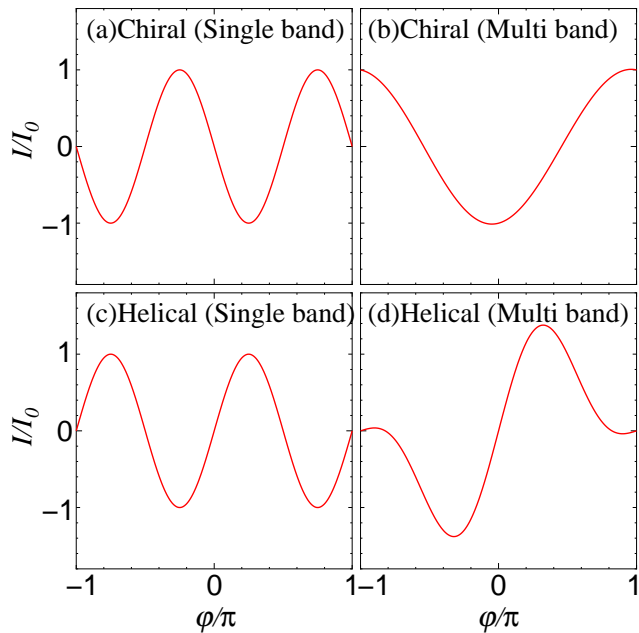


FIG. 2. Current-phase relation in the absence of interface Rashba spin-orbit interaction (λ_R) for (a) the chiral p -wave (E_u) in the single-band model, (b) the chiral p -wave (E_u) in the multi-band model, (c) the helical p -wave (A_{1u}) in the single-band model, and (d) the helical p -wave (A_{1u}) in the multi-band model

As shown in Figs. 2(a) and (c), the Josephson current is almost proportional to $\sin(2\varphi)$ in the case where the first-order Josephson coupling is absent. In fact, Table I shows that only the sinusoidal terms with an even-number order are nonzero. On the other hand, odd-order terms are nonzero in the case of the multi-band model, as shown in Fig. 2 and Table I (b) and (d). We confirmed that these odd-order terms are zero in the absence of spin-orbit interaction (LS coupling) in bulk SRO. We note that the cosine terms appear in the chiral p -wave case but are absent in the helical p -wave case. The cosine terms in the chiral p -wave case are nonzero even in the absence of Rashba spin-orbit coupling λ_R . This is because the hopping integral t_5 (*i.e.*, corresponding to inter-orbital hopping between the d_{yz} and d_{xz} orbitals) is nonzero and spin-orbit coupling in bulk SRO λ enhances the magnitude of the cosine terms. When the opposite chirality of the pair potential is chosen with

$$\begin{cases} \mathbf{d}_{E_u}^{yz} = \hat{z}\Delta_1(\delta \sin k_x - i \sin k_y), \\ \mathbf{d}_{E_u}^{zx} = \hat{z}\Delta_1(\sin k_x - i\delta \sin k_y), \\ \mathbf{d}_{E_u}^{xy} = \hat{z}\Delta_2(\sin k_x - i \sin k_y), \end{cases} \quad (30)$$

the signs of I_1^c and I_2^c are reversed.

We plot the current-phase relations in the presence of interface Rashba spin-orbit coupling ($\lambda_R > 0$) in Fig. 3. Figure 3 (c) shows no qualitative difference between the Josephson currents in the presence or absence of interface

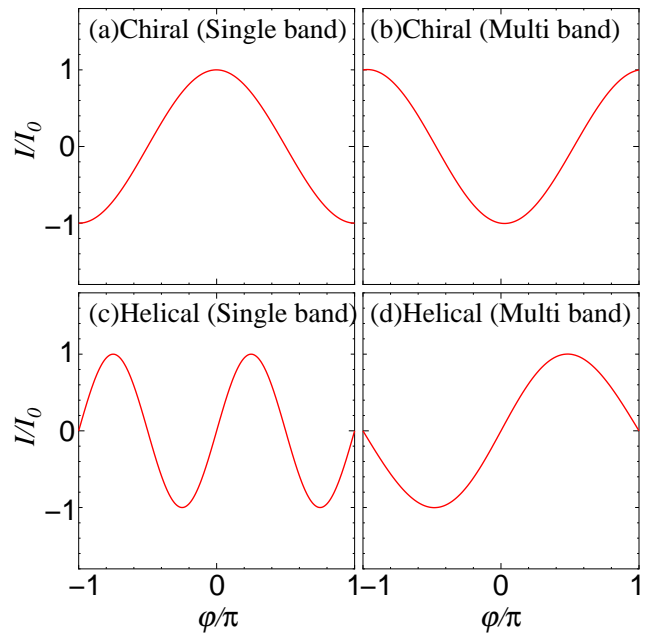


FIG. 3. Current-phase relation $I(\varphi)$ in the presence of interface Rashba spin-orbit interaction ($\lambda_R > 0$) for (a) the chiral p -wave (E_u) in the single-band model, (b) the chiral p -wave (E_u) in the multi-band model, (c) the helical p -wave (A_{1u}) in the single-band model, and (d) the helical p -wave (A_{1u}) in the multi-band model.

	I_1^s	I_1^c	I_2^s	I_2^c
(a) Chiral(single-band)	-	✓	✓	-
(b) Chiral(multi-band)	✓	✓	✓	✓
(c) Helical(single-band)	-	-	✓	-
(d) Helical(multi-band)	✓	-	✓	-

TABLE II. Fourier series of the current-phase relation in the presence of interface Rashba spin-orbit interaction

Rashba spin-orbit interaction, in the single-band model and in the case of helical pairing. On the other hand, cosine terms appear as a result of the interface Rashba spin-orbit coupling in the case of the chiral p -wave shown in Fig. 3 (a)⁶³. By contrast, there is no qualitative difference between the current-phase relations in the presence or absence of interface Rashba spin-orbit interaction in the multi-band model, as shown in Figs. 3 (b,d) and Table II (b,d). In the most general case, where both the interface Rashba spin-orbit interaction and bulk LS coupling in the multi-band model exist, we observe a qualitative difference between the chiral and helical p -wave cases. The cosine terms I_1^c and I_2^c appear only in the case of chiral p -wave pairing. This difference is due to the broken TRS that occurs in chiral p -wave pairing. In the following calculations for various junctions, we considered the interface Rashba spin-orbit interactions and used the multi-band model.

In order to take into account the corner structure of

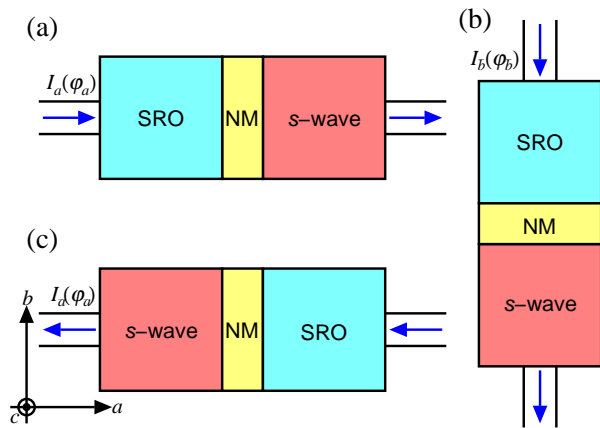


FIG. 4. Schematic illustrations of the SRO /NM/s-wave superconductor single Josephson junctions considered in this paper. Current-phase relations in junctions (a)-(c) were calculated independently. The results were then combined to calculate the magnetic-field dependence of the corner junction, corner SQUID, and symmetric SQUID.

Type of pairing	Relation between $I_a(\varphi_a)$ and $I_b(\varphi_b)$
Chiral(E_u)	$I_a(\varphi_a) = -I_b(-\varphi_b + \pi/2)$
Helical(A_{1u}, B_{2u})	$I_a(\varphi_a) = I_b(\varphi_b)$
Helical(A_{2u}, B_{1u})	$I_a(\varphi_a) = I_b(\varphi_b + \pi)$

TABLE III. Relations between $I_a(\varphi_a)$ and $I_b(\varphi_b)$ shown in Fig. 1 for chiral(E_u), helical (A_{1u}, B_{2u}), and helical (A_{2u}, B_{1u}) pairings.

the junction, we show the relation between the current phase relations in different orientations in Table III. The orientation dependence affects the maximum Josephson current in a corner junction or SQUID when it is written as a function of the external magnetic flux Φ . Although the calculation of the Φ dependence will be shown in next subsection, we first show the relation between $I_a(\varphi_a)$ and $I_b(\varphi_b)$ indicated in Fig. 4. This relation depends on the pairing symmetries specified in TABLE III. This relation in chiral p -wave pairing is different from that in helical p -wave pairing. Furthermore, in the helical p -wave cases, the relation between $I_a(\varphi_a)$ and $I_b(\varphi_b)$ depends on the irreducible representations of the pair potentials. This affects the properties of the corner junction or corner SQUID, as shown in the next subsection. Next, we show the relation between the $I_a(\varphi_a)$ and $I_b(\varphi_b)$ indicated in Fig. 1. The equation $I_a(\varphi) = I_b(\varphi + \pi)$ is valid for all pairings. This fact influences the properties of a symmetric SQUID.

B. Magnetic-field dependence of the maximum Josephson current in various junctions

In this subsection, we calculate the magnetic-field dependence of the maximum Josephson current in corner junctions, corner SQUIDS, and symmetric SQUIDS. We

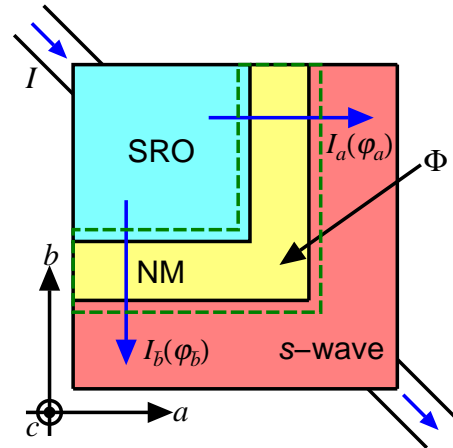


FIG. 5. Schematic illustration of an SRO/NM/s-wave corner junction

calculated the relation between the external magnetic flux Φ and the maximum Josephson current I_c by a standard method. In the Josephson junctions shown in Figs. 1 and 4, we assumed that the external magnetic field was applied parallel to the z -axis. The vector potential is then given by

$$\mathbf{A} = A_y(x)\mathbf{y}. \quad (31)$$

On the other hand, the phase γ of the pair potential obeys

$$\nabla\gamma = \frac{m^*\mathbf{v}_s}{\hbar} + \frac{2\pi}{\Phi_0}\mathbf{A}. \quad (32)$$

Since the magnetic field is screened inside the superconductor because of the Meissner effect, $A_y(x)$ takes the constant value $A_y(\infty)$ found at locations far from the interface. Using these properties, we integrated both sides of the y component of Eq. (32) with respect to y .

$$\gamma(y) = \gamma(0) + \frac{2\pi}{\Phi_0}A(\infty)y \quad (33)$$

The phase difference between the s -wave superconductor and the SRO is therefore given by

$$\varphi(y) = \varphi(0) + \frac{2\pi}{\Phi_0} [A_2(\infty) - A_1(\infty)]y. \quad (34)$$

Here, A_1 and A_2 represent the vector potentials far from the interface in the SRO and s -wave superconductor, respectively. The Fourier components of the Josephson current, I_n^s and I_n^c , defined in eq. (29), were obtained in the previous subsection in the absence of a magnetic field.

In the presence of a magnetic field, the Josephson current becomes a function of y . We integrated this function with respect to y :

$$I(\Phi, \varphi(0)) = Z \int_{-Y/2}^{Y/2} I(y) dy \quad (35)$$

$$= YZ \sum_{n=1}^{\infty} \left\{ \frac{\sin(n\pi\Phi/\Phi_0)}{n\pi\Phi/\Phi_0} [I_n^s \sin(n\varphi(0)) + I_n^c \cos(n\varphi(0))] \right\},$$

where, Y and Z are the sizes of the junction. It is evident that Eq.(35) displays a periodicity of 2π with respect to $\varphi(0)$. Therefore, by changing $\varphi(0)$ over the range $-\pi \leq \varphi(0) \leq \pi$, the maximum Josephson current I_c can be obtained as a function of the external magnetic flux Φ .

Next, we calculated the maximum Josephson current I_c in the corner junction shown in Fig. 5 as a function of Φ , using a similar approach to that described in [71]. We obtained the current-phase relations $I_a(\varphi_a)$ and $I_{\bar{b}}(\varphi_{\bar{b}})$ indicated in Fig. 5. By calculating the following equation instead of Eq. (35), we obtained the maximum Josephson current I_c as a function of the external magnetic flux Φ based on $I(\Phi, \varphi(0))$, given by

$$I(\Phi, \varphi(0)) = Z \left[\int_0^{Y/2} I_a(y) dy + \int_{-Y/2}^0 I_{\bar{b}}(y) dy \right].$$

Finally, we calculated the maximum Josephson current I_c as a function of the external magnetic flux Φ in the two types of SQUID shown in Fig. 6. The macroscopic phase differences of the two superconductors φ_a and $\varphi_{\bar{b}}$ obey the following relation:

$$\varphi_{\bar{b}} - \varphi_a = \frac{2\pi\Phi}{\Phi_0}. \quad (36)$$

The total current in these parallel circuits is therefore given by

$$I(\Phi, \varphi) = I_a(\varphi) + I_{\bar{b}}(\varphi + \frac{2\pi\Phi}{\Phi_0}). \quad (37)$$

By evaluating the maximum value of Eq. (37) for a given external magnetic flux Φ , we obtained the maximum Josephson current as a function of Φ .

Type of pairing	Φ dependence	zero points of $I(\Phi)$
(a) Chiral(E_u)	asymmetric	$\pm 2\Phi_0, \pm 4\Phi_0, \dots$
(b) Helical(A_{1u}, B_{2u})	symmetric	$\pm\Phi_0, \pm 2\Phi_0, \dots$
(c) Helical(A_{2u}, B_{1u})	symmetric	$\pm 2\Phi_0, \pm 4\Phi_0, \dots$

TABLE IV. Φ dependence and zero points of $I(\Phi)$ in an SRO/NM/s-wave corner junction for (b) chiral(E_u), (c) helical(A_{1u}, B_{2u}), and (d) helical(A_{2u}, B_{1u}) pairings in SRO. Schematic illustration of corner junction (a).

The I_c functions for the corner junction of SRO are plotted in Fig. 7. In the cases of the helical p -wave, the positions of the minima depend on the d -vector as shown in Figs. 5(b) and (c). This is because the relation between the Josephson currents $I_a(\varphi_a)$ and $I_{\bar{b}}(\varphi_{\bar{b}})$ in

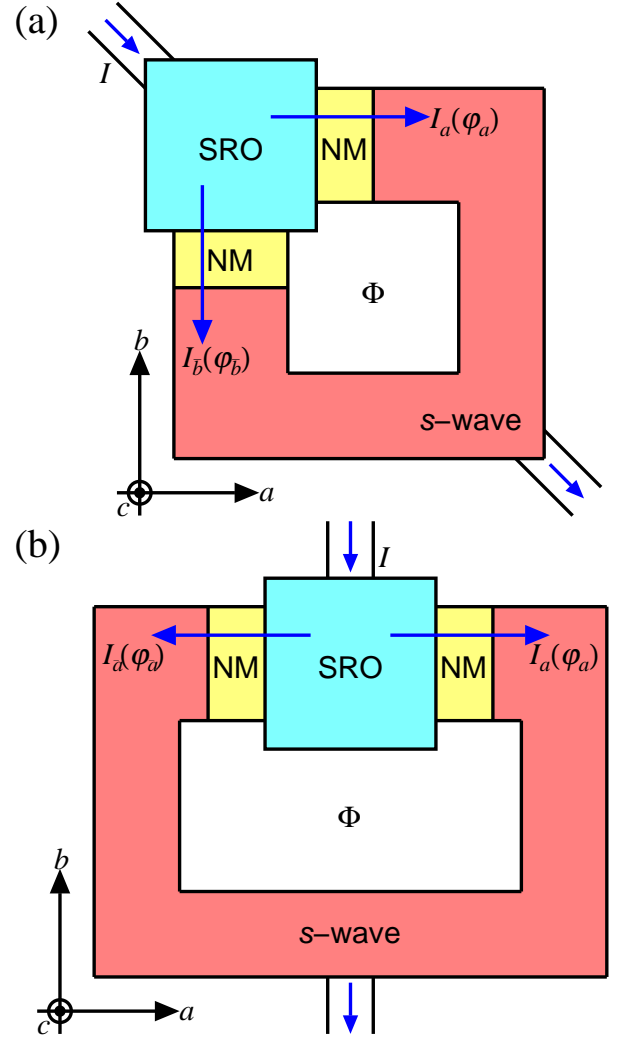


FIG. 6. Schematic illustration of SRO/NM/s-wave SQUIDs: (a) corner SQUID and (b) symmetric SQUID.

Fig. 7 is different for each pairing symmetry. In particular, $I_a(\varphi) = I_{\bar{b}}(\varphi)$ for the A_{1u} and B_{2u} pairings, while $I_a(\varphi) = I_{\bar{b}}(\varphi + \pi)$ for the A_{2u} and B_{1u} pairings. For all the helical p -wave cases, the Fraunhofer patterns are symmetric functions of Φ . On the other hand, $I(\Phi)$ is not a symmetric function of Φ for chiral p -wave pairing. This difference results from the existence of the cosine terms in the current-phase relation. In other words, the broken TRS causes the asymmetry of $I_c = I_c(\Phi)$, *i.e.*, $I_c(\Phi) \neq I_c(-\Phi)$. These results are summarized in Table IV. As seen from this table, there are qualitative differences between the helical and chiral p -wave pairings. The asymmetry of the Josephson current is due to the existence of cosine terms in the current-phase relation for the chiral p -wave pairings. These cosine terms can be nonzero unless both λ and λ_R are nonzero owing to the presence of inter-orbital hopping in the multi-band model. The magnitudes of these cosine terms and the re-

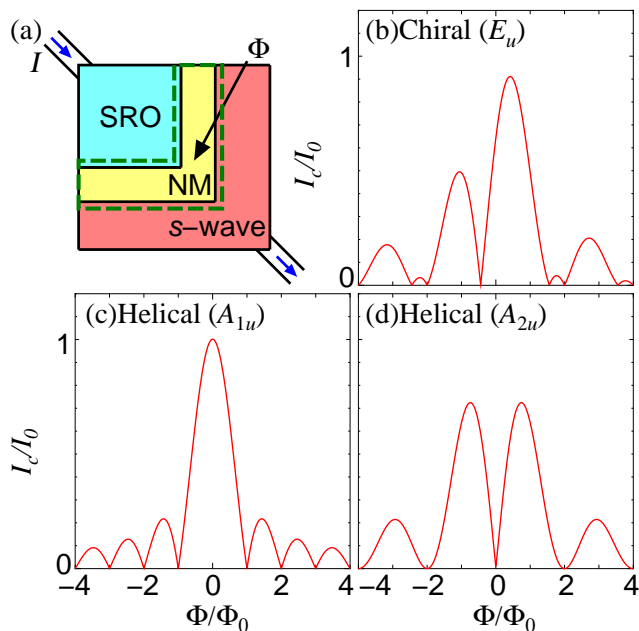


FIG. 7. Fraunhofer pattern in the SRO/NM/*s*-wave. (a) Schematic illustration of a corner junction, and the corresponding Fraunhofer pattern for (b) chiral (E_u) pairing, (c) helical (A_{1u}) pairing, and (d) helical (A_{2u}) pairing.

sulting asymmetry of $I(\Phi)$ are enhanced by the spin-orbit interactions, expressed through λ and λ_R .

Type of pairing	Φ dependence	Period
(a) Chiral	asymmetric	Φ_0
(b, c) Helical	symmetric	Φ_0

TABLE V. Φ dependence and period of the maximum Josephson current I_c in a corner SQUID

Next, we discuss I_c in the corner SQUID shown in Fig. 8. This I_c is symmetric or asymmetric with respect to Φ for the helical and chiral cases, respectively. As in the case of the SRO/NM/*s*-wave corner junction, the existence of the cosine terms in the current-phase relation in chiral pairing causes the asymmetry of $I_c(\Phi)$. The chiral pairing is consistent with a previous study based on a single-band model⁷². In the cases of helical pairing, the position of the maximum or minimum in $I_c(\Phi)$ depends on the pairing symmetry (irreducible representation), *i.e.*, the d -vector as shown in Figs. 8(b) and (c). We note that the Φ_0 periodicity in the helical pairing case appears only for a three-band model.

Finally, we consider the case of the so-called symmetric SQUID⁷³. Figure 9 shows the Φ dependence of I_c in the symmetric SQUID shown in Fig. 6(b). In this junction, there is no qualitative difference between the cases of chiral and helical pairing since $I_a(\varphi) = I_b(\varphi + \pi)$ is satisfied. The resulting Josephson current I_c is symmetric for both

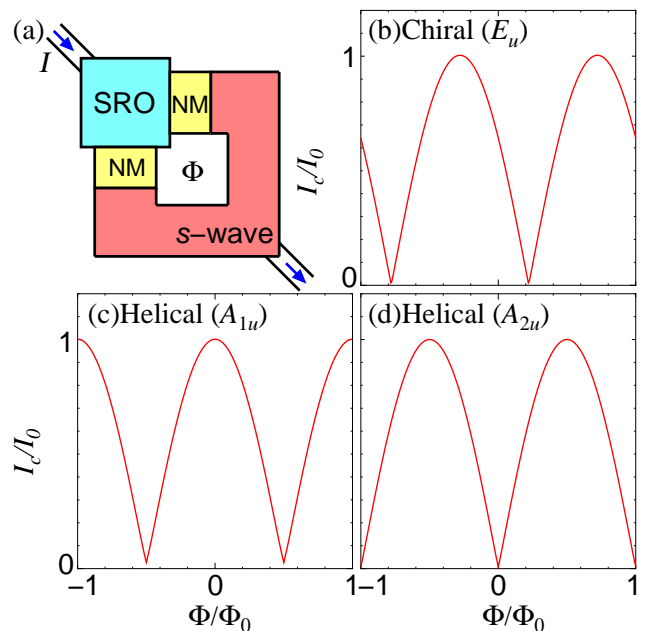


FIG. 8. (a) Maximum Josephson current I_c in a corner SQUID for (b) chiral (E_u), (b) helical (A_{1u}), and (c) helical (A_{2u}) pairings.

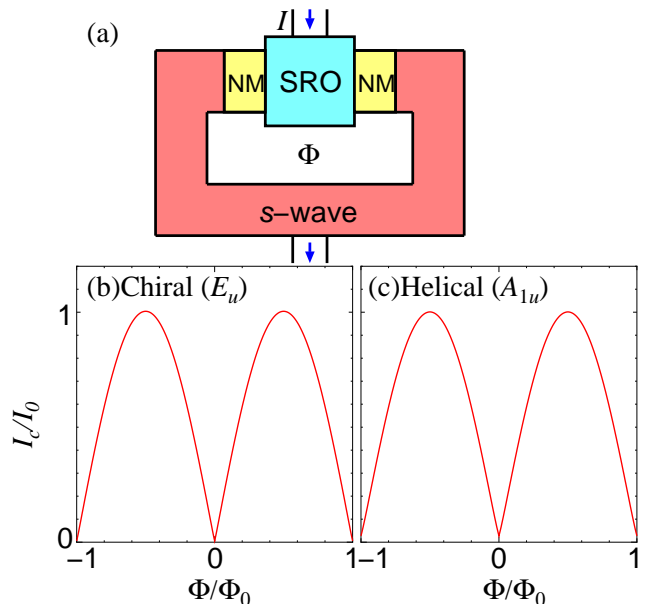


FIG. 9. (a) Symmetric SQUID and the corresponding I_c for (b) chiral (E_u) and (c) helical (A_{1u}) pairings

Type of pairing	Φ dependence	Period
(a) Chiral	symmetric	Φ_0
(b) Helical	symmetric	Φ_0

TABLE VI. Φ dependence and period of the maximum Josephson current I_c in a symmetric SQUID.

chiral and helical pairings, including in the presence of the cosine terms. Thus, we do not find any qualitative difference in I_c for the chiral and helical pairings in this symmetric SQUID.

IV. DISCUSSION AND SUMMARY

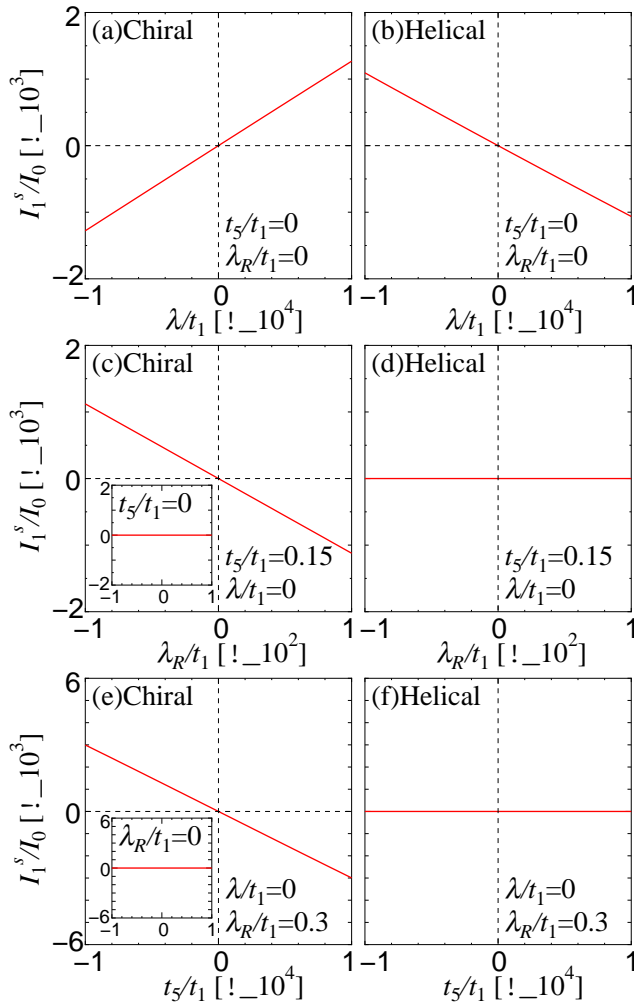


FIG. 10. I_1^s (the coefficient of $\sin(\varphi)$ in the Fourier series of the current-phase relation in the junction) is plotted as a function of λ (a, b), λ_R (c, d), and t_5 (e, f). Chiral pairing applies in (a), (c), and (e), and helical pairing with A_{1u} symmetry in (b), (d), and (f). $t_5 = 0$ and $\lambda_R = 0$ in (a) and (b). $t_5/t_1 = 0.15$ and $\lambda = 0$ in (c) and (d). $\lambda = 0$ and $\lambda/t_1 = 0.3$ in (e) and (f).

Here, we discuss the multi-band effect on the Josephson current in the present calculations, starting with the chiral p -wave case. As shown in TABLES I and II, the spin-orbit interaction in the bulk SRO (λ) and the interface Rashba spin-orbit interaction (λ_R) generate I_1^s for chiral p -wave pairing. We found that the coefficient of

the $\sin(\varphi)$ term I_1^s has the form

$$I_1^s = \alpha\lambda + \beta t_5 \lambda_R + O(\lambda^2) + O(t_5^2 \lambda_R^2), \quad (38)$$

which is confirmed by Fig. 10. This form suggests that λ directly induces I_1^s , whereas the existence of inter-orbital hopping t_5 is needed to produce I_1^s from λ_R . In the single-band model, I_1^s is absent while I_1^c is induced by λ_R in chiral p -wave pairing. In the multi-orbital model, t_5 induces the effective phase shift of the pair potential. A part of I_1^c is then converted to I_1^s by t_5 . Thus, we can conclude that the existence of I_1^s results from the multi-band model in SRO. This term becomes dominant in the limit of low transmissivities, where the higher-order Josephson couplings are strongly suppressed.

Next, we discuss the helical p -wave case, where I_1^s is given by

$$I_1^s = \alpha\lambda + O(\lambda^2). \quad (39)$$

This is because I_1^c does not exist in the single-band model owing to the TRS of the helical p -wave pairing. Since t_5 only gives the effective phase shift of the pair potential, I_1^s cannot be produced by λ_R . On the other hand, λ directly induces I_1^s in a similar manner as in the case of the chiral p -wave pairing.

In summary, we have studied Josephson currents in SRO/NM/ s -wave junctions. We found that the first-order Josephson coupling is induced by the spin-orbit interaction for the cases of both chiral and helical p -wave pairings. Note that the $\sin(\varphi)$ term, which is absent in the single-band model, appears as a result of the spin-orbit interaction and inter-band hopping. In the case of helical pairing, the first-order Josephson term appears only in the three-band model. Owing to the existence of the first-order Josephson coupling, the period of the Josephson current, as the magnetic flux Φ is varied, is expected to become the period of the conventional junctions. For the case of chiral p -wave pairing, the Josephson current shows asymmetric behavior in the corner junction and the corner SQUID, owing to broken TRS. This asymmetry is enhanced by the spin-orbit interaction in the bulk SRO or at the interface in the junction. Since the magnitude of the spin-orbit interaction in SRO is not very small, it is possible to detect the asymmetry experimentally if the TRS breaking by chiral pairing is realized.

In this paper, we assumed ballistic junctions with flat interfaces. Surface roughness and impurity scattering are known to influence charge transport in spin-triplet p -wave superconductor junctions^{74,75}. In particular, the odd-frequency spin-triplet s -wave component generated near the interface induces an anomalous proximity effect^{22,23}, and the resulting Josephson current displays a low-temperature anomaly²²⁻²⁴. Taking into account the impurity-scattering effect in the multi-band model is an interesting prospect for future work.

ACKNOWLEDGMENTS

This work was supported by a Grant-in-Aid for Scientific Research on Innovative Areas, Topological Material Science (Grants No. JP15H05851, No. JP15H05852, and No. JP15H05853), a Grant-in-Aid for Scientific Research B (Grant No. JP15H03686), a Grant-in-Aid for Chal-

lenging Exploratory Research (Grant No. JP15K13498) from the Ministry of Education, Culture, Sports, Science, and Technology, Japan (MEXT); Japan-RFBR JSPS Bilateral Joint Research Projects/Seminars (Grants No. 15-52-50054 and No. 15668956); Dutch FOM; the Ministry of Education and Science of the Russian Federation, Grant No. 14.Y26.31.0007; and by the Russian Science Foundation, Grant No. 15-12-30030.

-
- ¹ Y. Maeno, H. Hashimoto, K. Yoshida, S. Nishizaki, T. Fujita, J. G. Bednorz, and F. Lichtenberg, *Nature* **372**, 532 (1994).
- ² K. Ishida, H. Mukuda, Y. Kitaoka, K. Asayama, Z. Q. Mao, Y. Mori, and Y. Maeno, *Nature* **396**, 658 (1998).
- ³ H. Tou, Y. Kitaoka, K. Ishida, K. Asayama, N. Kimura, Y. Onuki, E. Yamamoto, Y. Haga, and Y. Maeno, *Phys. Rev. Lett.* **80**, 3129 (1998).
- ⁴ H. Murakawa, K. Ishida, K. Kitagawa, Z. Q. Mao, and Y. Maeno, *Phys. Rev. Lett.* **93**, 167004 (2004).
- ⁵ A. P. Mackenzie and Y. Maeno, *Rev. Mod. Phys.* **75**, 657 (2003).
- ⁶ Y. Maeno, S. Kittaka, T. Nomura, S. Yonezawa, and K. Ishida, *Journal of the Physical Society of Japan* **81**, 011009 (2012).
- ⁷ T. M. Rice and M. Sigrist, *Journal of Physics: Condensed Matter* **7**, L643 (1995).
- ⁸ K. Miyake and O. Narikiyo, *Phys. Rev. Lett.* **83**, 1423 (1999).
- ⁹ T. Kuwabara and M. Ogata, *Phys. Rev. Lett.* **85**, 4586 (2000).
- ¹⁰ T. Nomura and K. Yamada, *Journal of the Physical Society of Japan* **69**, 3678 (2000).
- ¹¹ T. Nomura and K. Yamada, *Journal of the Physical Society of Japan* **71**, 404 (2002).
- ¹² T. Nomura and K. Yamada, *Journal of the Physical Society of Japan* **71**, 1993 (2002).
- ¹³ R. Arita, S. Onari, K. Kuroki, and H. Aoki, *Phys. Rev. Lett.* **92**, 247006 (2004).
- ¹⁴ T. Nomura and K. Yamada, *Journal of the Physical Society of Japan* **74**, 1818 (2005).
- ¹⁵ T. Nomura, D. S. Hirashima, and K. Yamada, *Journal of the Physical Society of Japan* **77**, 024701 (2008).
- ¹⁶ Y. Yanase and M. Ogata, *Journal of the Physical Society of Japan* **72**, 673 (2003).
- ¹⁷ S. Raghu, A. Kapitulnik, and S. A. Kivelson, *Phys. Rev. Lett.* **105**, 136401 (2010).
- ¹⁸ M. Sato and M. Kohmoto, *Journal of the Physical Society of Japan* **69**, 3505.
- ¹⁹ K. Kuroki, M. Ogata, R. Arita, and H. Aoki, *Phys. Rev. B* **63**, 060506 (2001).
- ²⁰ T. Takimoto, *Phys. Rev. B* **62**, R14641 (2000).
- ²¹ M. Tsuchiizu, Y. Yamakawa, S. Onari, Y. Ohno, and H. Kontani, *Phys. Rev. B* **91**, 155103 (2015).
- ²² Y. Tanaka and S. Kashiwaya, *Phys. Rev. B* **70**, 012507 (2004).
- ²³ Y. Tanaka, S. Kashiwaya, and T. Yokoyama, *Phys. Rev. B* **71**, 094513 (2005).
- ²⁴ Y. Asano, Y. Tanaka, and S. Kashiwaya, *Phys. Rev. Lett.* **96**, 097007 (2006).
- ²⁵ Y. Tanaka, Y. Asano, A. Golubov, and S. Kashiwaya, *Phys. Rev. B* **72**, 140503(R) (2005).
- ²⁶ Y. Tanaka and A. A. Golubov, *Phys. Rev. Lett.* **98**, 037003 (2007).
- ²⁷ A. P. Schnyder, S. Ryu, A. Furusaki, and A. W. W. Ludwig, *Phys. Rev. B* **78**, 195125 (2008).
- ²⁸ X.-L. Qi and S.-C. Zhang, *Rev. Mod. Phys.* **83**, 1057 (2011).
- ²⁹ Y. Tanaka, M. Sato, and N. Nagaosa, *J. Phys. Soc. Jpn.* **81**, 011013 (2012).
- ³⁰ J. Alicea, *Rep. Prog. Phys.* **75** (2012).
- ³¹ S. Kashiwaya, H. Kashiwaya, H. Kambara, T. Furuta, H. Yaguchi, Y. Tanaka, and Y. Maeno, *Phys. Rev. Lett.* **107**, 077003 (2011).
- ³² K. D. Nelson, Z. Q. Mao, Y. Maeno, and Y. Liu, *Science* **306**, 1151 (2004).
- ³³ F. Laube, G. Goll, H. v. Löhneysen, M. Fogelström, and F. Lichtenberg, *Phys. Rev. Lett.* **84**, 1595 (2000).
- ³⁴ H. Wang, W. Lou, J. Luo, J. Wei, Y. Liu, J. E. Ortman, and Z. Q. Mao, *Phys. Rev. B* **91**, 184514 (2015).
- ³⁵ A. Furusaki, M. Matsumoto, and M. Sigrist, *Phys. Rev. B* **64**, 054514 (2001).
- ³⁶ K. Sengupta, H.-J. Kwon, and V. M. Yakovenko, *Phys. Rev. B* **65**, 104504 (2002).
- ³⁷ M. Yamashiro, Y. Tanaka, and S. Kashiwaya, *Phys. Rev. B* **56**, 7847 (1997).
- ³⁸ M. Yamashiro, Y. Tanaka, Y. Tanuma, and S. Kashiwaya, *J. Phys. Soc. Jpn.* **67**, 3224 (1998).
- ³⁹ C. Honerkamp and M. Sigrist, *Journal of Low Temperature Physics* **111**, 895 (1998).
- ⁴⁰ Y. Tanaka and S. Kashiwaya, *Phys. Rev. Lett.* **74**, 3451 (1995).
- ⁴¹ S. Kashiwaya and Y. Tanaka, *Rep. Prog. Phys.* **63**, 1641 (2000).
- ⁴² C. R. Hu, *Phys. Rev. Lett.* **72**, 1526 (1994).
- ⁴³ Y. Imai, K. Wakabayashi, and M. Sigrist, *Phys. Rev. B* **85**, 174532 (2012).
- ⁴⁴ Y. Imai, K. Wakabayashi, and M. Sigrist, *Phys. Rev. B* **88**, 144503 (2013).
- ⁴⁵ K. Yada, A. A. Golubov, Y. Tanaka, and S. Kashiwaya, *Journal of the Physical Society of Japan* **83**, 074706 (2014).
- ⁴⁶ F. Kidwingira, J. D. Strand, D. J. Harlingen, and Y. Maeno, *Science* **314**, 1267 (2006).
- ⁴⁷ H. Kambara, S. Kashiwaya, H. Yaguchi, Y. Asano, Y. Tanaka, and Y. Maeno, *Phys. Rev. Lett.* **101**, 267003 (2008).
- ⁴⁸ H. Kambara, T. Matsumoto, H. Kashiwaya, S. Kashiwaya, H. Yaguchi, Y. Asano, Y. Tanaka, and Y. Maeno, *Journal of the Physical Society of Japan* **79**, 074708 (2010).
- ⁴⁹ M. S. Anwar, T. Nakamura, S. Yonezawa, M. Yakabe, R. Ishiguro, H. Takayanagi, and Y. Maeno, *Sci. Rep.* **3**, 2480 (2013).

- ⁵⁰ K. Saitoh, S. Kashiwaya, H. Kashiwaya, Y. Mawatari, Y. Asano, Y. Tanaka, and Y. Maeno, *Phys. Rev. B* **92**, 100504 (2015).
- ⁵¹ X.-L. Qi, T. L. Hughes, S. Raghu, and S.-C. Zhang, *Phys. Rev. Lett.* **102**, 187001 (2009).
- ⁵² M. Matsumoto and M. Sigrist, *Journal of the Physical Society of Japan* **68**, 3120 (1999).
- ⁵³ S.-I. Suzuki and Y. Asano, *Phys. Rev. B* **94**, 155302 (2016).
- ⁵⁴ G. M. Luke, Y. Fudamoto, K. M. Kojima, M. I. Larkin, J. Merrin, B. Nachumi, Y. J. Uemura, Y. Maeno, Z. Q. Mao, Y. Mori, H. Nakamura, and M. Sigrist, *Nature* **394**, 558.
- ⁵⁵ J. Xia, Y. Maeno, P. T. Beyersdorf, M. M. Fejer, and A. Kapitulnik, *Phys. Rev. Lett.* **97**, 167002 (2006).
- ⁵⁶ J. R. Kirtley, C. Kallin, C. W. Hicks, E.-A. Kim, Y. Liu, K. A. Moler, Y. Maeno, and K. D. Nelson, *Phys. Rev. B* **76**, 014526 (2007).
- ⁵⁷ C. W. Hicks, J. R. Kirtley, T. M. Lippman, N. C. Koshnick, M. E. Huber, Y. Maeno, W. M. Yuhasz, M. B. Maple, and K. A. Moler, *Phys. Rev. B* **81**, 214501 (2010).
- ⁵⁸ W. Huang, E. Taylor, and C. Kallin, *Phys. Rev. B* **90**, 224519 (2014).
- ⁵⁹ S. Lederer, W. Huang, E. Taylor, S. Raghu, and C. Kallin, *Phys. Rev. B* **90**, 134521 (2014).
- ⁶⁰ P. E. C. Ashby and C. Kallin, *Phys. Rev. B* **79**, 224509 (2009).
- ⁶¹ Y. Tada, N. Kawakami, and S. Fujimoto, *New Journal of Physics* **11**, 055070 (2009).
- ⁶² T. Nomura and K. Yamada, *Journal of the Physical Society of Japan* **74**, 1818 (2002).
- ⁶³ Y. Asano, Y. Tanaka, M. Sigrist, and S. Kashiwaya, *Phys. Rev. B* **67**, 184505 (2003).
- ⁶⁴ T. Oguchi, *Phys. Rev. B* **51**, 1385 (1995).
- ⁶⁵ D. J. Singh, *Phys. Rev. B* **52**, 1358 (1995).
- ⁶⁶ C. Noce and M. Cuoco, *Phys. Rev. B* **59**, 2659 (1999).
- ⁶⁷ M. W. Haverkort, I. S. Elfimov, L. H. Tjeng, G. A. Sawatzky, and A. Damascelli, *Phys. Rev. Lett.* **101**, 026406 (2008).
- ⁶⁸ A. Furusaki and M. Tsukada, *Solid State Communications* **78**, 299 (1991).
- ⁶⁹ Y. Tanaka and S. Kashiwaya, *Phys. Rev. B* **56**, 892 (1997).
- ⁷⁰ A. Umerski, *Phys. Rev. B* **55**, 5266 (1997).
- ⁷¹ D. J. Van Harlingen, *Rev. Mod. Phys.* **67**, 515 (1995).
- ⁷² Y. Asano, Y. Tanaka, M. Sigrist, and S. Kashiwaya, *Phys. Rev. B* **71**, 214501 (2005).
- ⁷³ V. B. Geshkenbein, A. I. Larkin, and A. Barone, *Phys. Rev. B* **36**, 235 (1987).
- ⁷⁴ S. V. Bakurskiy, A. A. Golubov, M. Y. Kupriyanov, K. Yada, and Y. Tanaka, *Phys. Rev. B* **90**, 064513 (2014).
- ⁷⁵ B. Lu, P. Bursset, Y. Tanuma, A. A. Golubov, Y. Asano, and Y. Tanaka, *Phys. Rev. B* **94**, 014504 (2016).